Supporting information
Integrated CO_2 Capture and Conversion as an Efficient Process for Fuels from Greenhouse Gases

Sung Min Kim,[†] Paula M. Abdala,[†] Marcin Broda,[†] Davood Hosseini,[†]
Christophe Copéret,[‡] and Christoph Müller*[,†]

[†]Department of Mechanical and Process Engineering, ETH Zürich, Leonhardstrasse 21, 8092 Zürich, Switzerland

[‡] Department of Chemistry and Applied Sciences, ETH Zürich, Vladimir Prelog Weg 1-5, 8093 Zürich, Switzerland

correspondence to: muelchri@ethz.ch (Prof. Christoph Müller)

Content

Supplementary Text 3

Table S1. Physicochemical properties of reacted Ni/MgO-Al_2O_3 DRM catalyst 4

Figures 5

Figure S1. Schematic diagram of a conventional calcium looping based CO_2 capture process. 5

Figure S2. Schematic diagram of the fluidized bed setup. 5

Figure S3. H_2-TPR profile of Ni/MgO-Al_2O_3 6

Figure S4. Characterization of the reacted DRM catalyst: (a) X-ray powder diffraction patterns: (△) periclase (MgO), (◇) Ni, and (×) graphite. (b) Raman spectra and TEM of the reacted DRM catalyst after (c) the 1st and (d) the 10th cycle. 7

Figure S5. (a) CH_4 and CO_2 conversion and (b) yield of H_2 and CO, and H_2/CO ratio in the pre-breakthrough stage as a function of the cycle number. 8

Figure S6. Molar flow rate of H_2 and CO during CO_2 conversion (DRM) and subsequent CO_2 capture at different cycle numbers: (——) 1st, (- - -) 5th and (– · –) 10th cycle 8

Figure S7. Characterization of the reacted CO_2 sorbent: HR-SEM images of (a) reacted limestone after the 10th cycle (calcined form), and (b) BJH pore size distribution of the freshly calcined and reacted limestone. 9

Figure S8. (a) CO_2 release profile for 3 g of limestone at 900 °C and (b) regeneration of limestone coupled with DRM reaction at 900 °C. 9

Figure S9. N_2 physisorption isotherms of calcined limestone and reduced Ni/MgO-Al_2O_3. 10

References 10

Supplementary Text

Material characterization

Due to the hygroscopic nature of the material, $Ca(OH)_2$ is also observed in the XRD patterns of the material after calcination (Figure2e). N_2 physisorption measurements (FigureS9) reveal that calcined limestone has a macro-porous morphology with a type III isotherm and H3 type hysteresis loop (IUPAC classification [1]), a BET surface area of 16 $m^2/g_{sorbent}$ and a BJH pore volume and pore diameter of 0.13 $cm^3/g_{sorbnet}$ and 38.2 nm, respectively.

Turning to the dry reforming catalyst, after reduction at 800 °C (the reduction temperature was determined by H_2-TPR experiments, FigureS2), Ni/MgO-Al_2O_3 (Figure2e) contains metallic nickel and periclase phases (MgO-Al_2O_3). The XRD data shows that the d(200) spacing of periclase in reduced DRM catalyst (2.093 Å) is smaller than that of the pure periclase reference, MgO, (2.102 Å), indicative that Al^{3+} cations are incorporated into the periclase structure [2]. N_2 physisorption measurements show a type IV isotherm and a H2 type hysteresis loop, indicating a mesoporous morphology (BET surface area and BJH pore volume was equal to 163 $m^2/g_{catalyst}$ and 0.91 $cm^3/g_{catalyst}$, respectively). Using H_2 chemisorption, a Ni surface area of 10.3 $m^2 \cdot g_{cat}^{-1}$ is determined.

Cyclic CO_2 capture performance of limestone-derived CaO as determined in a TGA

To rationalize the cyclic CO_2 capture capacity measured in the fluidized bed (Figure4b), the cyclic CO_2 uptake of limestone-derived CaO is also evaluated in a TGA at 720 °C. Although there are appreciable difference between a TGA and a fluidized bed e.g. with regards to mass transfer characteristics, we find that CO_2 capacity of limestone-derived CaO as determined in a TGA is comparable to the results obtained in a fluidized bed. This observation indicates that for the given number of cycles, attrition is a minor contributor to the decreasing CO_2 uptake of limestone.

Regeneration of $CaCO_3$ coupled with DRM at 900 °C

We tests the regeneration of $CaCO_3$ under pure CH_4 stream at 900 °C after CO_2 capture at 720 °C. 3 g of pre-calcined limestone is used to avoid complete calcination of $CaCO_3$ before reaching at 900 °C. The CO_2 molar fraction was reached to 0.49 under N_2 (0.2 L/min) at 900 °C, albeit very short (≈ 3 min) due to limited quantity of $CaCO_3$ (FigureS8a). The coupled CO_2 capture and conversion reactions at 900 °C using a mixture of 3.0 g limestone and 3.0 g Ni/MgO-Al_2O_3 is performed (FigureS8b) under pure CH_4 (0.2 L/min). H_2 mole fraction is prominently high due to CH_4 decomposition (t = 25 – 31 min), where CO_2 released from $CaCO_3$ is completely converted CO and CO mole fraction was gradually increased in accordance with CO_2 release profile of $CaCO_3$ depending on temperature. Only H_2 and CO with 1.04 of H_2/CO molar ratio is observed in pre-breakthrough at 900 °C (t = 30 – 33 min), indicative of full conversion of the CO_2 released

via the dry reforming of methane into a synthesis. In breakthrough, CO mole fraction is steadily reduced due to the quantity of CO_2 released decreased, whereas H_2 mole fraction is increased due to CH_4 decomposition. In the post-breakthrough stage (t > 35 min), the concentration of CH_4 increases due to catalyst poisoning by carbon deposition and the depletion of $CaCO_3$.

Table S1. Physicochemical properties of reacted Ni/MgO-Al_2O_3 DRM catalyst

Catalyst	H_2 chemisorption	N_2 physisorption[b]		
	Ni active site[a] [$\mu mol_{Ni}/g_{cat}$]	S_{BET} [m^2/g_{cat}]	V_p [$cm^3/gcat$]	D_p [nm]
Freshly reduced	262	163	0.91	5.2
1st post-breakthrough	10	142	0.75	5.9
2nd carbonation	255	158	0.88	5.7
10th carbonation	210	155	0.87	5.9
10th post-breakthrough	8	133	0.72	5.9

[a] Ni active sites quantified by H_2 chemisorption using a stoichiometry factor of H/Ni = 1.0. [b]The specific surface area, pore volume, and pore radius were calculated using BET and BJH models.

Figures

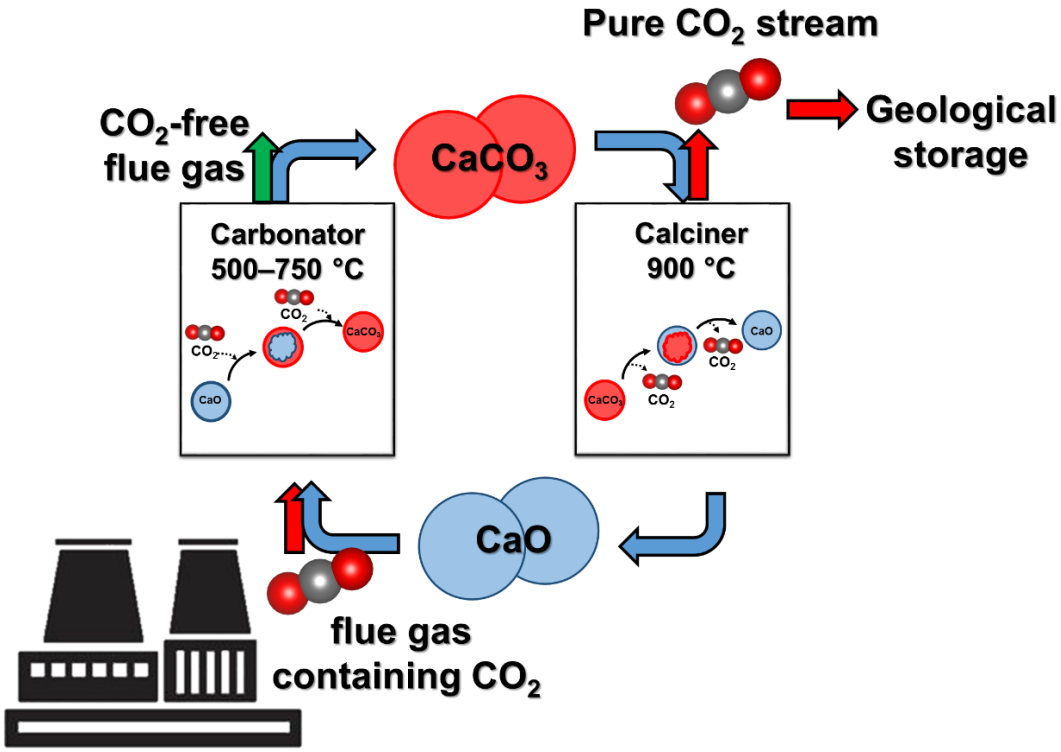

Figure S1. Schematic diagram of a conventional calcium looping based CO_2 capture process.

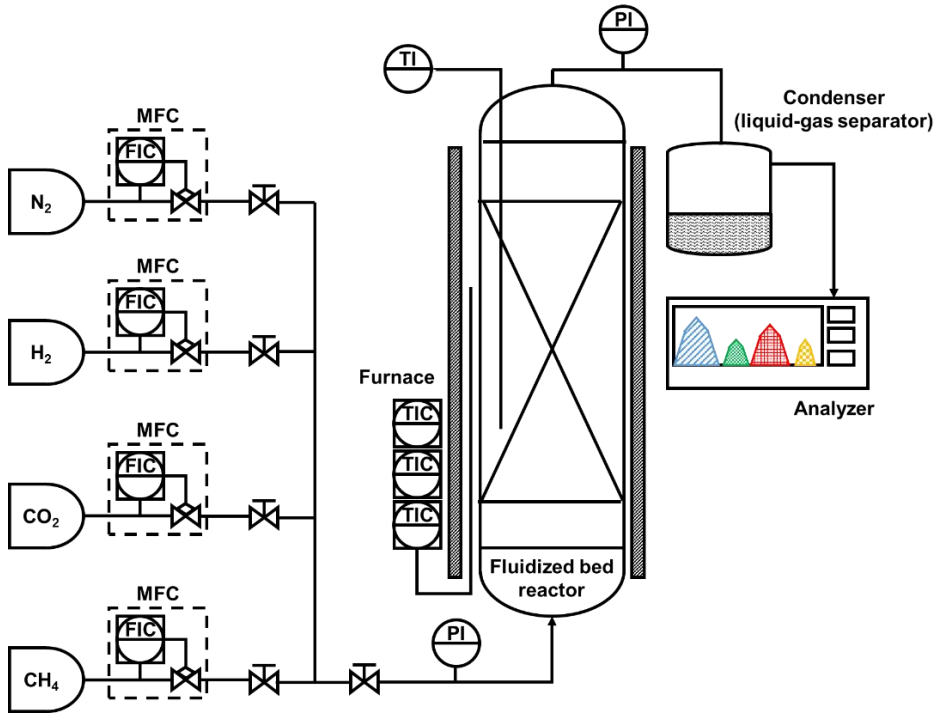

Figure S2. Schematic diagram of the fluidized bed setup.

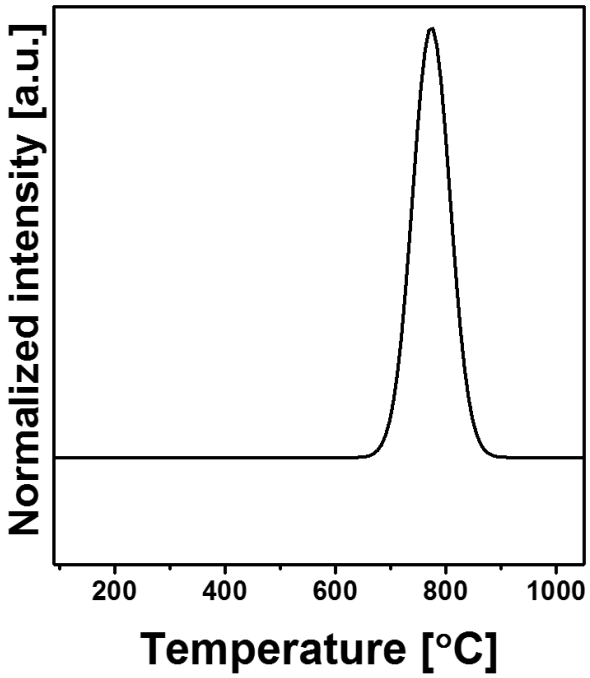

Figure S3. H_2-TPR profile of Ni/MgO-Al_2O_3

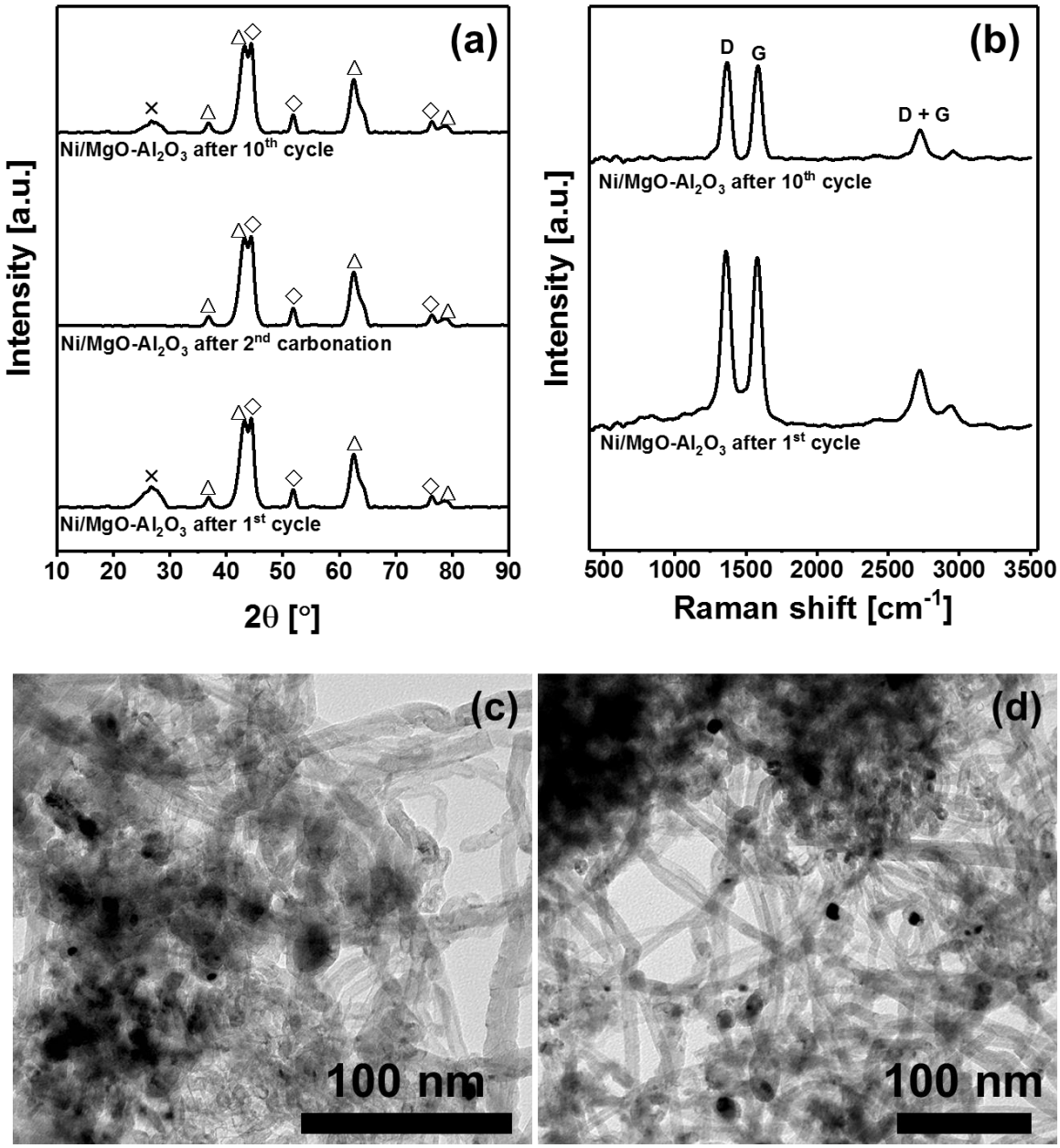

Figure S4. Characterization of the reacted DRM catalyst: (a) X-ray powder diffraction patterns: (△) periclase (MgO), (◇) Ni, and (×) graphite. (b) Raman spectra and TEM of the reacted DRM catalyst after (c) the 1st and (d) the 10th cycle.

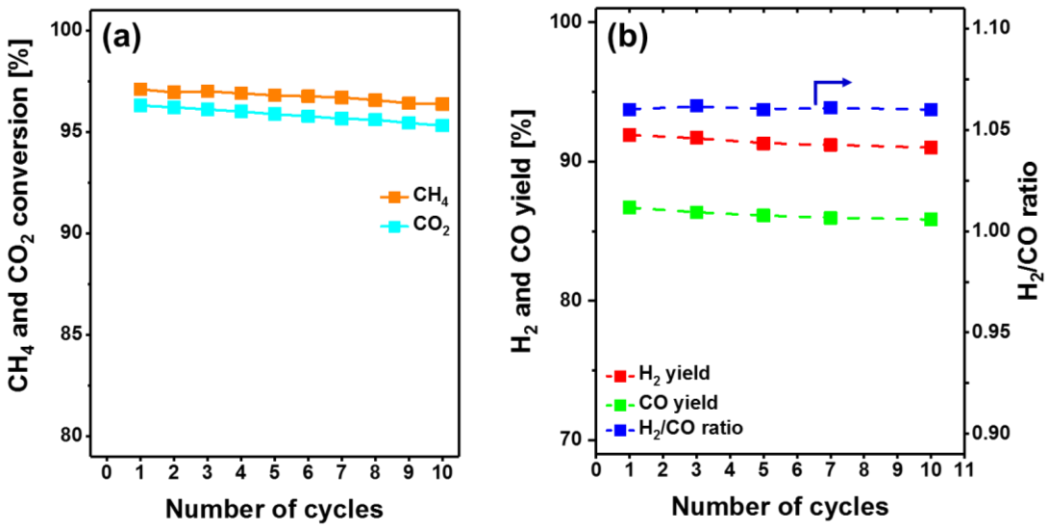

Figure S5. (a) CH_4 and CO_2 conversion and (b) yield of H_2 and CO, and H_2/CO ratio in the pre-breakthrough stage as a function of the cycle number.

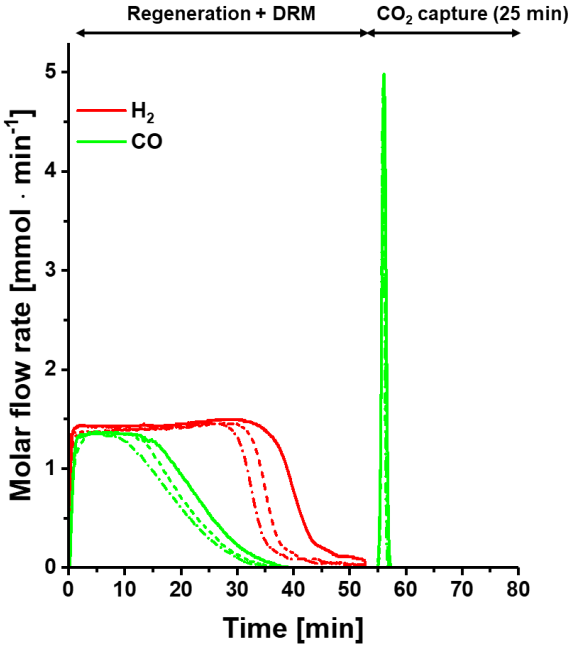

Figure S6. Molar flow rate of H_2 and CO during CO_2 conversion (DRM) and subsequent CO_2 capture at different cycle numbers: (——) 1st, (- - -) 5th and (– · –) 10th cycle

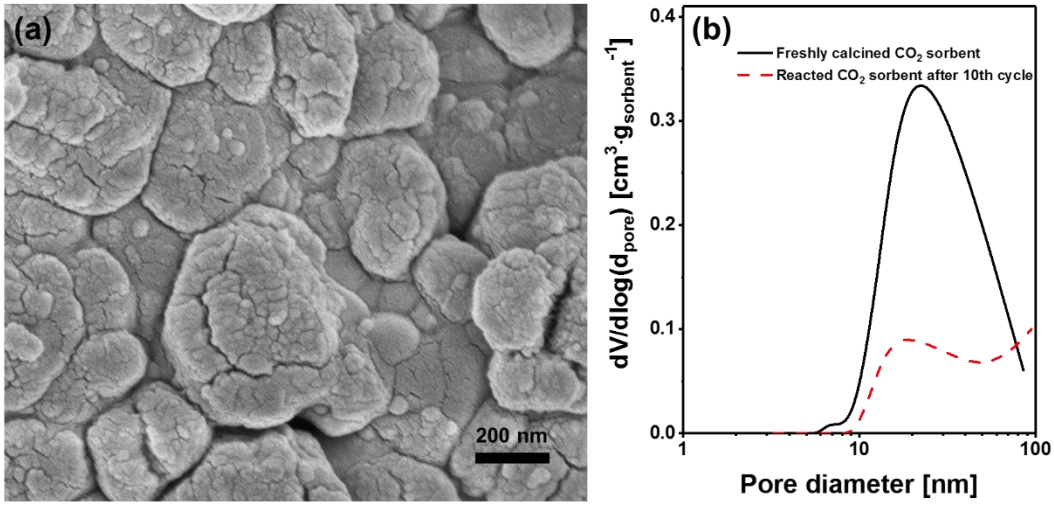

Figure S7. Characterization of the reacted CO_2 sorbent: HR-SEM images of (a) reacted limestone after the 10th cycle (calcined form), and (b) BJH pore size distribution of the freshly calcined and reacted limestone.

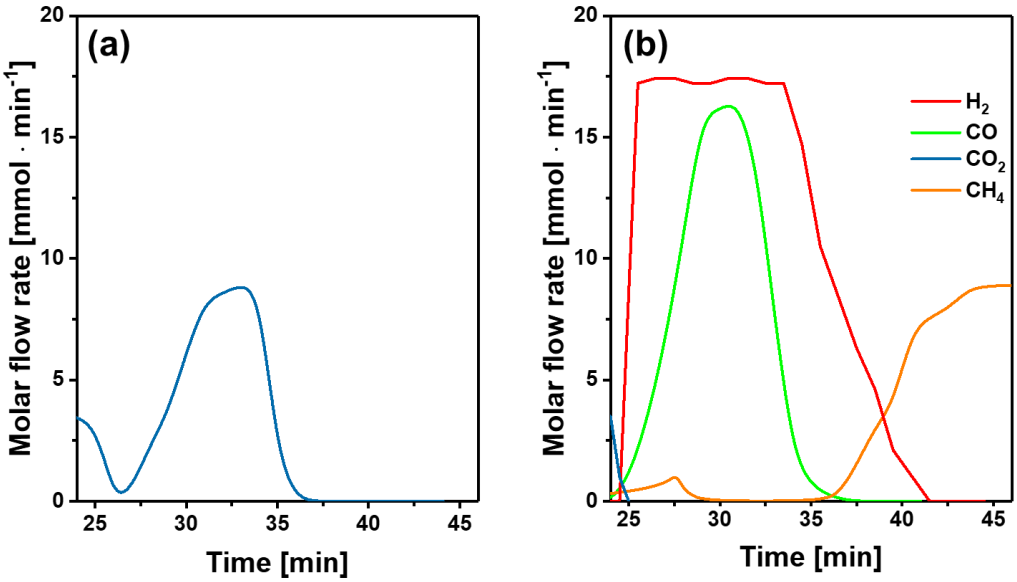

Figure S8. (a) CO_2 release profile for 3 g of limestone at 900 °C and (b) regeneration of limestone coupled with DRM reaction at 900 °C.

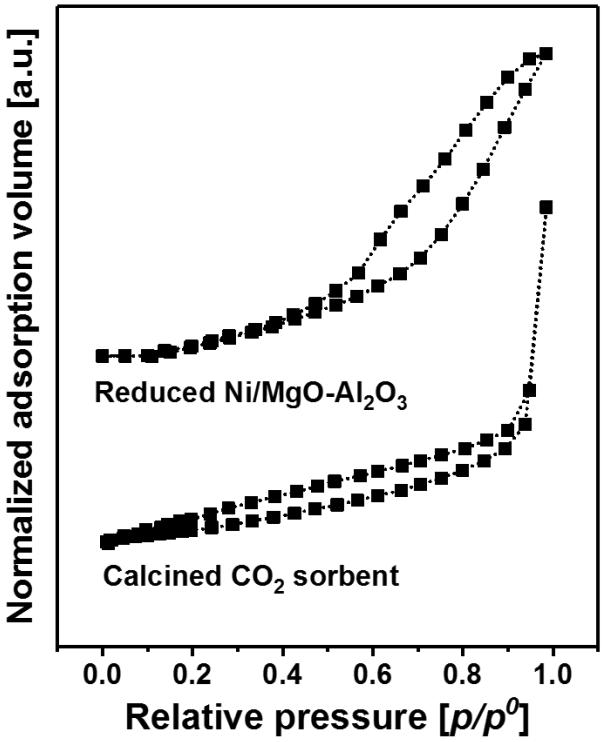

Figure S9. N_2 physisorption isotherms of calcined limestone and reduced Ni/MgO-Al_2O_3.

References

(1) Thommes, M.; Kaneko, K.; Neimark, A. V.; Olivier, J. P.; Rodriguez-Reinoso, F.; Rouquerol, J.; Sing, K. S., Pure Appl. Chem. **2015,** *87*, 1051-1069.

(2) Prescott, H. A.; Li, Z.-J.; Kemnitz, E.; Trunschke, A.; Deutsch, J.; Lieske, H.; Auroux, A., J. Catal. **2005,** *234*, 119-130.